Hindawi
Advances in Condensed Matter Physics
Volume 2018, Article ID 7598978, 10 pages
https://doi.org/10.1155/2018/7598978

Research Article

Structural and Optical Properties of Amorphous Al_2O_3 Thin Film Deposited by Atomic Layer Deposition

Shuzheng Shi,[1,2] **Shuo Qian**,[1] **Xiaojuan Hou**,[1] **Jiliang Mu**,[1] **Jian He**,[1] **and Xiujian Chou**[1]

[1]*Science and Technology on Electronic Test and Measurement Laboratory, North University of China, Taiyuan, China*
[2]*School of Mechanical Engineering, Hebei University of Architecture, Zhangjiakou, China*

Correspondence should be addressed to Jian He; drhejian@nuc.edu.cn and Xiujian Chou; chouxiujian@nuc.edu.cn

Received 6 December 2017; Accepted 24 January 2018; Published 6 March 2018

Academic Editor: Shicai Xu

Aluminum oxide (Al_2O_3) amorphous structure with short-range order and long-range disorder has presented promising applications in optical and optoelectronic devices. In this paper, the Al_2O_3 films with different thickness were prepared by atomic layer deposition (ALD) technology at 200°C in order to achieve amorphous structure. X-ray diffraction (XRD) and energy dispersive spectrum (EDS) results indicated that the Al_2O_3 films were amorphous structure and stable O/Al ratio. The surface topography investigated by atomic force microscopy (AFM) showed that the samples were smooth and crack-free. Spectroscopic ellipsometer (SE) measurements were operated to investigate the effect of thickness on the structure and optical properties of films with Tauc-Lorentz model. It is found that the band gap exhibits a steady value ~2.3 eV by the UV-VIS transmittance method, but the T-L model was ~3.0 eV. The refractive index and extinction coefficient are related to the variation of thickness and the samples surface quality of amorphous network structure in the thin films. The outstanding optoelectronic properties and facile fabrication of Al_2O_3 films amorphous structure can be extended to other similar oxides, which could display wide applications in various engineering and industrial fields.

1. Introduction

Aluminum oxide (Al_2O_3) is a technologically promising material in optics, machinery, batteries, and microelectronics applications because of its advantages like high dielectric constant, excellent stability, favorable thermal conductivity, high hardness, and low refractive index [1]. Al_2O_3 film can be fabricated by several methods, including chemical vapor deposition [2], electron beam evaporation [3], magnetron sputtering [4], the sol-gel process [5], pulsed laser deposition [6], and atomic layer deposition [7]. Among these techniques, Atomic Layer Deposition (ALD), a low-temperature atomic chemical vapor deposition technique, has advantages in homogeneity, compactness, precise composition, and thickness controllability of the target material on Ågstrom or monolayer level [8, 9]. Therefore, ALD is one of the most effective methods used in Al_2O_3 film fabrication, especially the application in optical lenses, refractory coatings, microelectronic devices, anticorrosive coatings, heat sinks in integrated circuits, and the passivation of metal surfaces. Al_2O_3 has complex and variable lattice structures based on the strong Al-O bonds and the atomic spatial sequence. When deposited on below 400°C, the Al_2O_3 films form amorphous structure with "short-range order and long-range disorder" [9, 10]. Amorphous Al_2O_3 plays an important role in optical applications like optical lenses and windows, antireflection coatings, and optical wave guides. As we know, a certain property of material originates from its special atomic structures. However, the complication in amorphous matrix and its sensitivity to process conditions makes it very difficult to control or predict the material performance. Therefore, a detailed investigation on the optical and structural properties of amorphous Al_2O_3 thin films is crucial to the improvement of device performance. In the last few decades, although there exist numerous related reports about crystalline Al_2O_3 film, the research on the

optical and structural properties of amorphous counterpart is rare.

In this paper, the effect of structure evolution on the optical properties of amorphous Al_2O_3 films deposited by ALD has been examined. By means of X-Ray Diffraction and Scanning Electron Microscopy-Energy Dispersive Spectrometer, the atomic configuration, the surface morphology, and the element composition were characterized. Furthermore, the optical properties of samples were analyzed by spectroscopic ellipsometer (SE) in spectral range [300 nm, 800 nm]. The ellipsometer spectra were fitted by Tauc-Lorentz dispersion model. The ultraviolet and visible transmission spectrum were used to confirm the band gap evolution and support the SE results. This investigation enables a better understanding of the structural and optical properties of amorphous Al_2O_3 films, also providing a new reference for other similar materials.

2. Experimental Method

2.1. Samples Preparation. A single crystal silicon substrate was used as the substrate for Al_2O_3 films growth, with 4 inches' N type, ⟨100⟩ crystalline phase, 375 μm, and resistivity of 1–10 Ω·cm. The glass wafer was cut into 1×1 cm^2. The Si and glass substrates were cleaned by acetone, anhydrous ethanol, and deionized water for 15 minutes to remove the organic impurities and the "stain trap" of the substrate surface, ensuring the purity and compliance of the Al_2O_3 film with silicon wafer. Then, the substrates were heated on the heating plate to remove excessive water in the temperatures of 300°C.

In the experiment, Al_2O_3 films were deposited on Si and glass substrates by ALD (TFS-200, Bene, Finland). Trimethylaluminum (TMA; ($Al(CH_3)_3$)) and H_2O were used as the precursor of metallic aluminum and oxygen ions. Simultaneously, high purity N_2 (99.999%) was used as the carrier and purge gas. To ensure the vacuum of the reaction chamber, the pressure differences about 3 Torr between internal and external chamber were controlled. The reacting temperature remained constant at 200°C. The Al_2O_3 films were deposited on silicon wafer and glass for 100, 200, 300, 400, and 500 cycles, respectively. TMA and H_2O were alternately entrained in the N_2 carrier flow using gas switching valves. The N_2 carrier gas pressure was 2.0 Torr. Each ALD cycle was as follows: 0.2 s to pulse TMA, 0.2 s to pulse H_2O as the second reactant, 2 s and 3 s to purging the chamber with high purity N_2 in 1st and 2st. Total time of a deposition cycle is 5.4 s.

2.2. Characterization and Measurement Methods. The film crystal structure was examined by X-ray diffraction (XRD, X'Pert PRO, PANalytical B.V., Netherlands). The compositions were evaluated by Scanning Electron Microscopy-Energy Dispersive Spectrometer (SEM-EDS, Zeiss 1450VP Scanning Electron Microscope). The roughness and surface topography were characterized by atomic force microscopy (AFM; Bruker Dimension Icon VT-1000, Santa Barbara, CA, USA). The optical properties of Al_2O_3 films were investigated by spectroscopic ellipsometer (SE, SENTECH SE850 UV/VIS/NIR, spectroscopic ellipsometer, Germany), of which the wavelength ranges from 300 to 800 nm at the incident angle of 65°. Besides, the ultraviolet-visible spectra were examined with ultraviolet and visible spectrophotometer (UV, SHIMADZU UV-1700 ultraviolet and visible spectrophotometer) which can extract the band gap evolution to support the SE results.

2.3. Spectroscopic Ellipsometer Principle of Measurement. When a beam of light enters a membrane at a certain angle, the thickness and optical parameters of the film can be determined by the polarization state variations of reflected light and transmitted light.

The ellipsometric parameters ψ and Δ are defined by the ellipsometric ratio ρ as the following equation [11]:

$$\rho = \frac{R_p}{R_s} = \left|\frac{R_p}{R_s}\right| e^{i(\Delta_p - \Delta_s)} = \tan\psi \exp\left(j\Delta\right), \tag{1}$$

where R_p and R_s are complex Fresnel reflection coefficients for "p" and "s" polarization, respectively. Δ_p and Δ_s represents the phase for each polarization. Ellipsometry measures the two values ψ and Δ, which express the amplitude ratio and phase difference between p polarization and s polarization, shown in (1). Based on the above calculation, dielectric function of film can be expressed as

$$\varepsilon = \varepsilon_1 + \varepsilon_2 = \varepsilon_0 \sin^2\phi_0 \left[1 + \tan^2\phi_0 \left(\frac{1-\rho}{1+\rho}\right)^2\right], \tag{2}$$

where ϕ_0, ε_0 represent the incident angle and the vacuum dielectric function, respectively.

In this case, the refractive index n and extinction coefficient k can be extracted from the two ellipsometry parameters. For single layer film, the amplitude ratio ψ is characterized by the refractive index n, while Δ represents light absorption by applying the Fresnel equations. The ellipsometer fitting iterative are evaluated by an objective optimization function [11, 12]. The mean square deviation can be described by Root Mean Square Error (RMSE) between the theoretical and experimental value, which is given as follows:

$$\text{RMSE} = \sqrt{\frac{1}{2N - M - 1} \sum_{i=1}^{N} \left[\left(\psi_i^{\text{cal}} - \psi_i^{\text{exp}}\right)^2 + \left(\Delta_i^{\text{cal}} - \Delta_i^{\text{exp}}\right)^2\right]}, \tag{3}$$

where N is the number of measured wavelengths, M is the number of variables, ψ_i^{cal} and Δ_i^{cal} represent the theoretical values, and ψ_i^{exp} and Δ_i^{exp} are experimental measurements, respectively. When the RMSE value is less than 1, the fitting results are reliable [11–13].

3. Results and Discussion

3.1. Crystal Structure and Compositional Analysis. The intensity of XRD is sensitive to the atomic arrangement of material, so it is capable of analyzing crystal structure. Figure 1 gives the XRD patterns of naked Si substrate and deposited films with

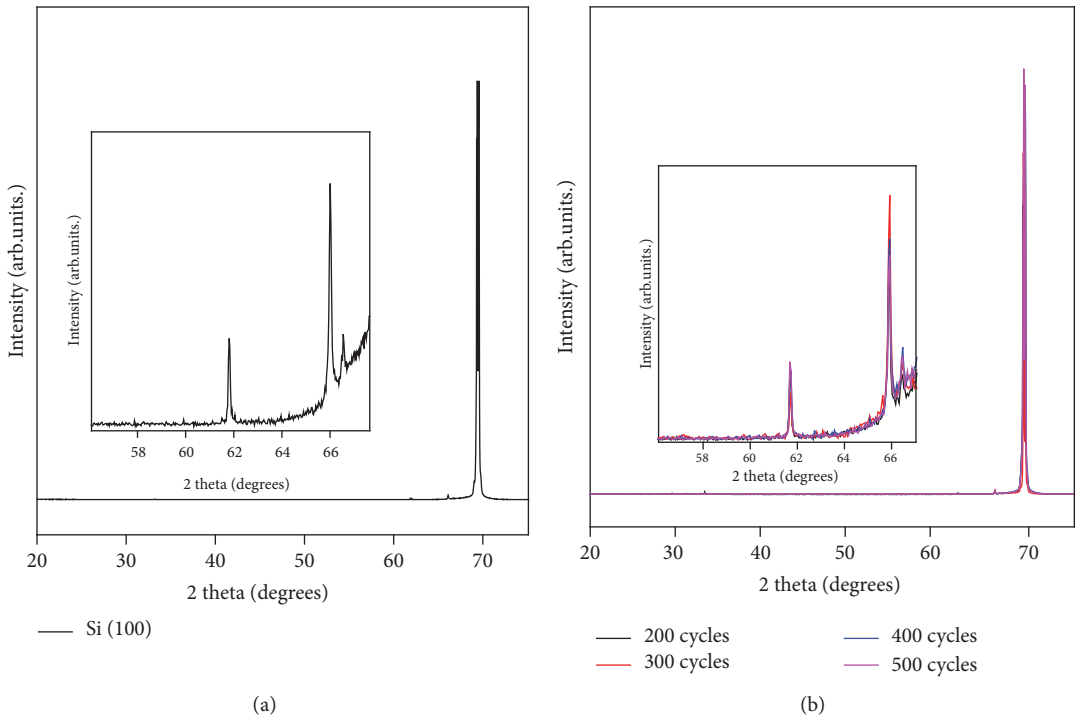

Figure 1: XRD patterns of Si (100) and all films of different cycles grown on Si (100) substrates.

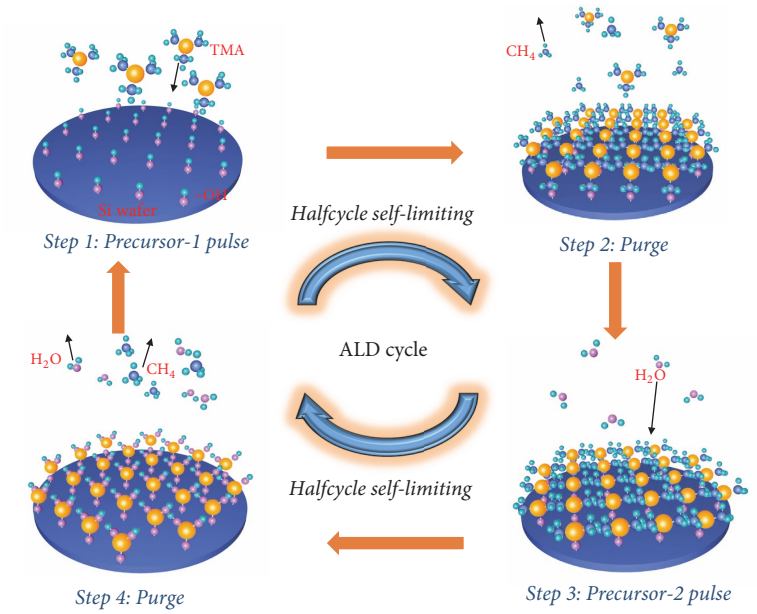

Figure 2: ALD process schematic.

different cycles. It can be seen from Figure 1(a) that Si XRD exhibits three diffraction peaks at 61.86°, 66.02°, and 69.16°, respectively. Likewise, the XRD patterns of all deposited films almost completely overlap the Si XRD [14], and no other peaks are observed, implying the amorphous structure of the obtained samples.

In ALD, the monolayer deposition and the alternating precursor pulse can guarantee an excellent film deposition quality and uniform rate [7, 8]. Figure 2 shows the whole reaction cycle consisting of four steps. (1) Precursor TMA vapor is pulsed into the reaction chamber, and the chemical adsorption reaction 4 occurs on the surface of the substrate. (2) Excess precursor TMA and reaction by-products CH_4 are purged with inert carrier gas N_2. (3) Precursor deionized H_2O vapor is pulsed into the reaction chamber, the surface chemical reactions 4 is proceeded on surface of the adsorption by

Table 1: EDS data of different cycles Al_2O_3 film on silicon wafer (oxygen, aluminum, and silicon (%); the total = 100%).

ALD cycles	Elements	Wt.%	At. (%)	d (nm)	O/Al ratio
100	O	2.3	3.97	11.62	——
	Al	0	0		
	Si	97.7	96.03		
200	O	4.05	6.90	19.63	4.964029
	Al	1.38	1.39		
	Si	94.57	91.71		
300	O	5.85	9.82	30.95	5.223404
	Al	1.89	1.88		
	Si	92.27	88.30		
400	O	7.97	13.18	39.05	4.592334
	Al	2.93	2.87		
	Si	89.1	83.95		
500	O	11.23	18.15	50.40	5.385757
	Al	3.52	3.37		
	Si	85.25	78.48		

TMA. (4) Excess precursor H_2O and reaction by-products CH_4 are purged with inert carrier gas N_2.

The surface chemistry reaction for ALD-Al_2O_3 can be expressed as

$$\mathrm{Al(CH_3)_3\,(g) + Al\text{-}OH^*\,(s) \longrightarrow Al\text{-}O\text{-}Al(CH_3)_2{}^*\,(s) + CH_4\,(g)} \quad (A)$$

$$\mathrm{Al(CH_3)^*\,(s) + H_2O\,(s) \longrightarrow Al\text{-}OH^*\,(s) + CH_4\,(g)} \quad (B)$$

The overall reaction is

$$\mathrm{2Al(CH_3)_3\,(g) + 3H_2O\,(s) \longrightarrow Al_2O_3\,(s) + 6CH_4\,(g)} \quad (C)$$

$*$ refers to the functional groups adsorbed on the deposition surface, showing that self-stop gas-solid reaction is the basis of ALD. TMA/H_2O ALD process can be divided into 4 and 4 two half reactions, and the precursor molecule performs the chemical adsorption firstly on the deposition surface in each half reaction. Through ligand exchange between TMA and surface hydroxyl groups form the bridging oxygen bonds Al-O-Al on the surface and in the meantime release methane molecules. The reaction between the precursor and the deposition surface is chemical adsorption, the monolayer adsorption, which is also related to the steric hindrance of methyl groups. Therefore, the gas-solid surface reactions of ALD include adsorption, chemical reactions and desorption, and other processes.

The chemical composition of the films was evaluated using SEM-EDS. As shown in Table 1, result indicates that the atomic ratio O/Al in all samples is around 5, which is different from the value 1.5 in crystalline state [15]. In the report of Kääriäinen and Cameron [16], the O/Al value varies between 2.5 and 3.6 due to some oxygen ion contribution from precursor O_2. Gupta and Saleh [17] demonstrated that it is almost impossible to precisely control the atomic ratio in metal oxides, because some oxygen contribution comes from the oxygen-containing functional groups, such as carbonyl or carboxyl groups, on the growth surface. In our case, there are a large number of carbonyl groups adsorbed on the growth surface during reaction process leading to increased oxygen contribution because of the precursor H_2O shown in Figure 2. In addition, due to the limitation of SEM-EDS measurement accuracy, the extremely low Al content in the sample with 10.5833 nm of thickness cannot be detected. The EDS result combined with XRD result confirms that our samples deposited at 200°C is amorphous.

3.2. Morphological Analysis. The film surface quality has a direct influence on the optical and electrical performance of device, such as the optical scattering and electrical contact. Therefore, a precise control of surface morphology during film growth process is very crucial to device performance. In this work, AFM is used to characterize the surface structure of the amorphous Al_2O_3 films. Figure 3 gives the AFM results of Al_2O_3 film with different ALD cycles. The AFM scan is carried out on a 3 μm × 3 μm area with the tapping mode.

The surface morphologies of all samples are smooth and crack-free with similar root mean square (RMS) surface roughness values, which indicates that Al_2O_3 films were well fabricated. In order to study the cause of different growth rates of those of 50 cycles, we also studied the growth rate of films with ALD cycles below 50. The ALD surface reactions are very efficient, and Steps 1 and 3 are also known as the half reaction with the self-limitation and complementarity, while the self-limiting reaction is determined by the saturation adsorption of the group and the number of surface activated groups. Each group has a certain size, and the bonding location is blocked by adjacent chemical group, so the remaining groups can only be adsorbed in the next cycle. The number of surface activation groups determines the number of molecules per cycle. The Al_2O_3 films growth occurs during alternating exposures to TMA and H_2O. The main driver for the efficient reactions is the formation of a very strong Al-O bond. The films tend to be smooth and pinhole-free because the randomness of the

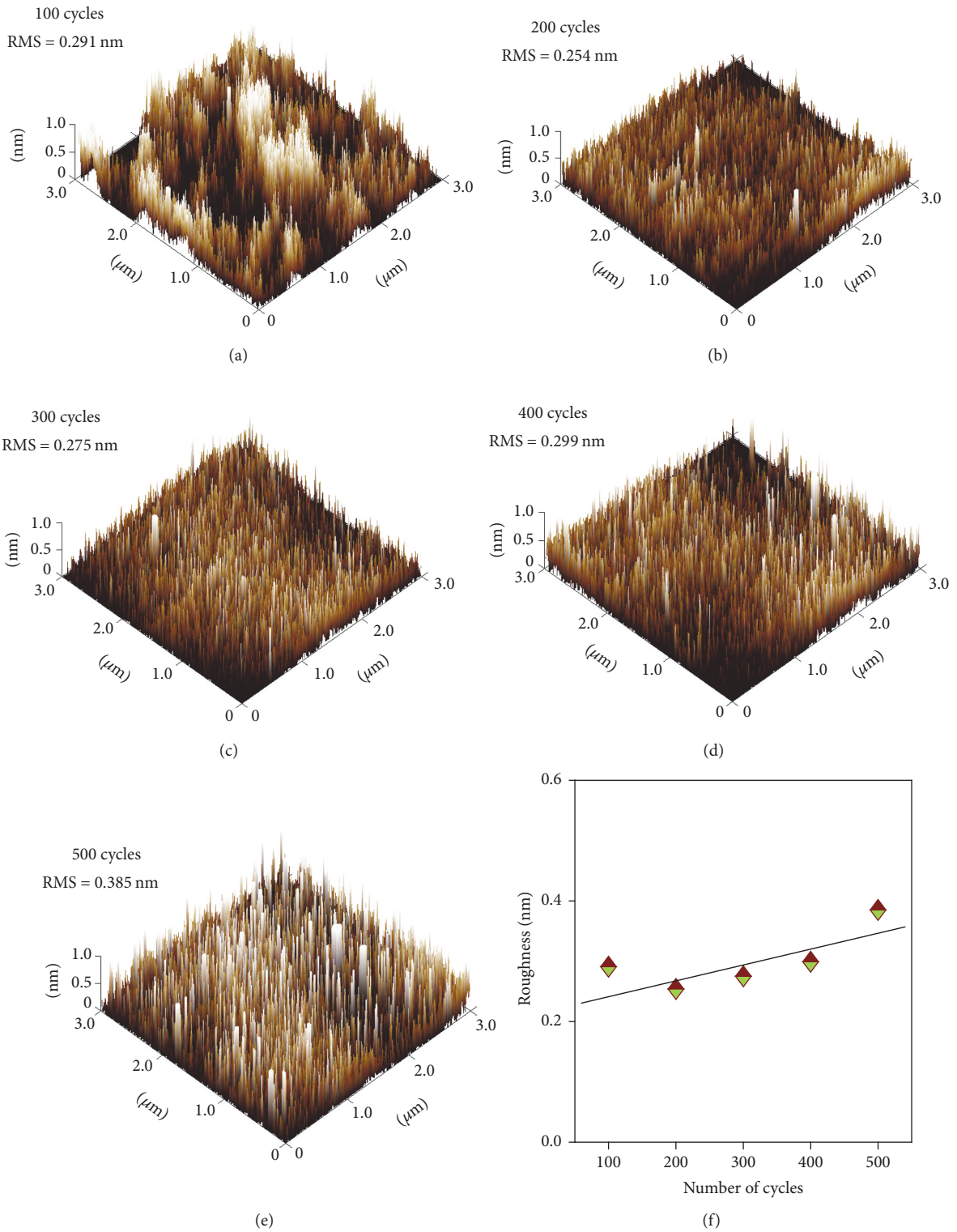

Figure 3: AFM micrographs of deposited Al_2O_3 films with different thicknesses. (a) 100 cycles. (b) 200 cycles. (c) 300 cycles. (d) 400 cycles. (e) 500 cycles. (f) Trend chart of roughness for the five samples. RMS represents root mean square roughness.

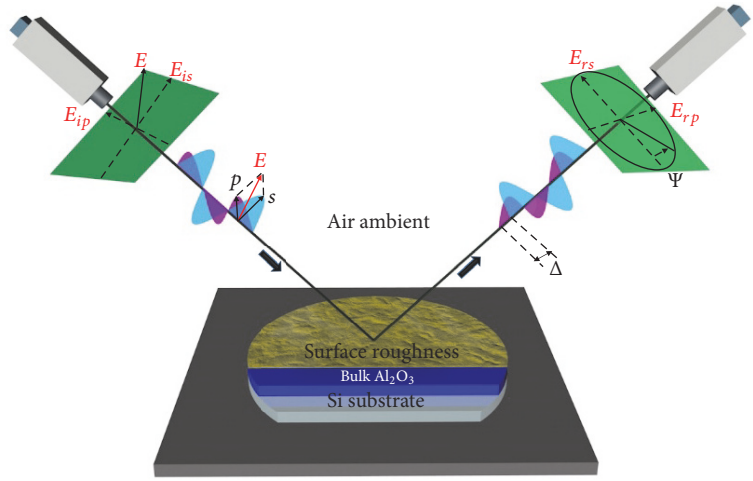

FIGURE 4: Spectroscopic ellipsometer schematic of Al_2O_3 film micronanosystem.

precursor flux and the self-limiting of the surface reactions. The reaction dose, deposition temperature, and so forth have little or no effect on the reaction. Thus, the growth rate is constant in the ALD process, which is insensitive to changes in process parameters, and the deposited films have excellent thickness uniformity and three-dimensional conformity.

3.3. Optical Property Analysis. Spectroscopic ellipsometer (SE) is an important thin film measurement technology for its nondestructive and sensitive advantages [18]. It is necessary to develop a proper optical model for the SE measurement and thus the extraction of optical and structural parameters. Our optical model for fit analysis is established as follows: Si substrate/bulk Al_2O_3 layer/surface roughness/air ambient, as shown in Figure 4. The surface roughness layer was modeled as a mixture of 50% bulk Al_2O_3 layer and 50% voids based on the Bruggeman effective medium approximation (EMA). Meanwhile, a reasonable material dispersion relationship is required during ellipsometry analysis. In our measurement, the Tauc-Lorentz model has been used. It is established by Jellison et al. in 1996 based on combined density and Lorentz oscillator model and more suitable for amorphous thin film compared to FB model [18, 19]. This model is defined as follows:

$$\varepsilon_1(E) = \varepsilon_1(\infty) + \frac{2}{\pi} P \int_{E_g}^{\infty} \frac{\tau \varepsilon_2(\tau)}{\tau^2 - E^2} d\tau,$$

$$\varepsilon_2(E) = \begin{cases} \dfrac{ACEE_0}{\left(E^2 - E_0^2\right)^2 + C^2E^2} \dfrac{\left(E - E_g\right)}{E^2} & \text{for } E > E_g, \\ 0 & \text{for } E \le E_g, \end{cases} \quad (4)$$

where P represents the Cauchy principal value of the integral. The dielectric function of the films is determined by five parameters [A, C, E_0, E_g, and $\varepsilon_1(\infty)$]. In the T-L model, ε_2 is modeled as the product of Tauc gap and Lorentz oscillator and ε_1 is derived by the Kramers–Kronig relations.

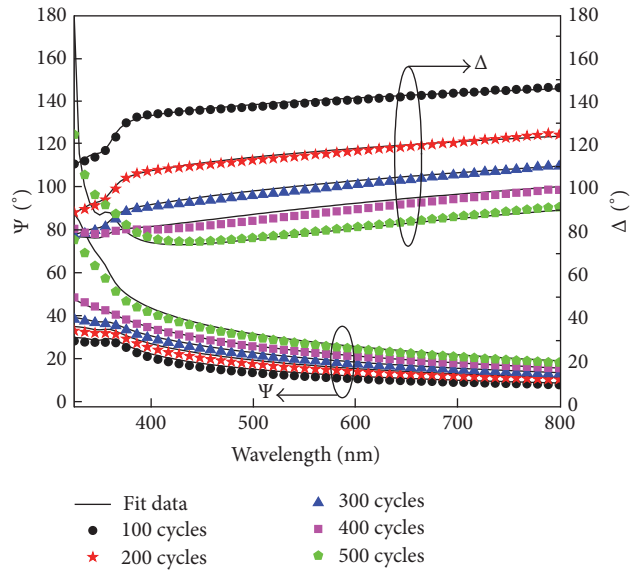

FIGURE 5: Al_2O_3 films ellipsometry spectra of fit data (continued curves) and measured data (gauge points).

The ellipsometry spectra of Al_2O_3 thin film with different ALD cycles have been obtained using the above theoretical model. Since the related parameters of all samples are extracted from Ψ and Δ fits, we give both the experimental and calculated data, respectively, as shown in Figure 5. The fitting parameters are listed in Table 2. It can be seen that the calculated outcomes fit the experimental points well. The objective function value f_{RMSE} in all samples is less than 1, demonstrating the acceptable optimization in our case.

SE measurement shows that the fundamental structural parameter, film thickness, increases regularly with the increase of ALD cycles, corresponding to a growth rate of ~0.1 nm/cycle. The relationship between thickness and cycle can be described by a linear fit function $d = 0.097n_c + 1.2328$ nm, as shown in Figure 6. As we know, SE analysis is an

Table 2: Structural and electronic parameters extracted from SE analysis of the five different samples.

ALD cycle	ε_1 (∞)	A	C	E_0/eV	E_g/eV	d/nm	d_s/nm	f_{RMSE}
100	1.66	118.24	644.70	74.33	3.08	11.62	0.08	0.68
200	1.39	156.83	393.56	70.30	2.99	19.63	0.25	0.67
300	1.22	72.65	39.07	25.23	2.98	30.95	0.89	0.58
400	0.59	334.78	430.62	92.86	2.92	39.05	0.15	0.53
500	1.11	207.70	295.86	59.76	2.92	50.40	0.21	0.73

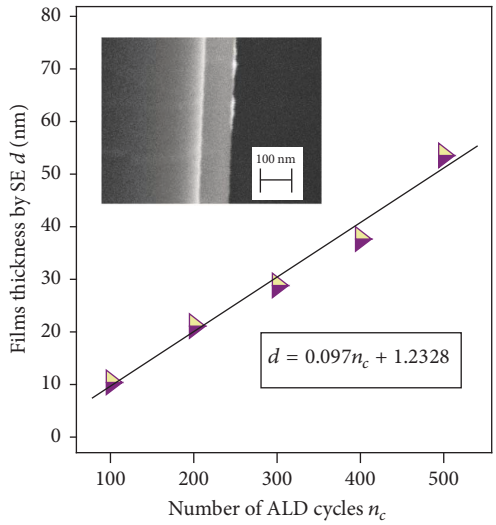

Figure 6: Trend chart of thickness for the five different cycle samples. The inset is SEM image of 1000 cycles ALD-Al_2O_3 film, where d and n_c represent film thickness and number of ALD cycles, respectively.

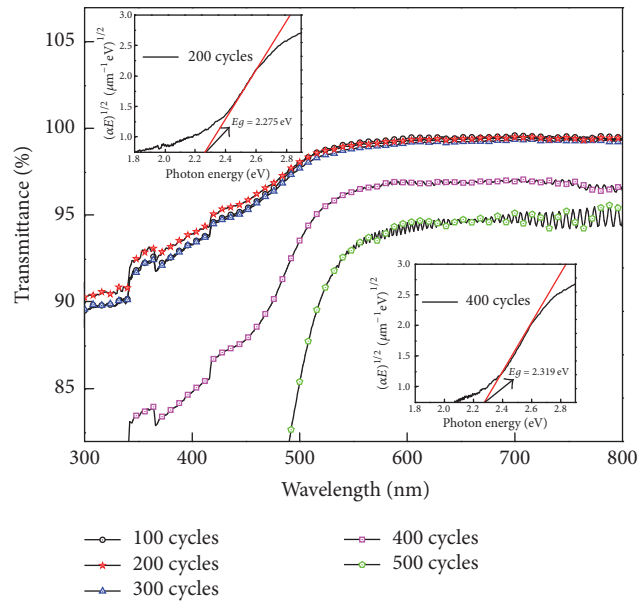

Figure 7: Optical transmittance spectra by UV-VIS transmittance measurement. The inset shows the optical band gaps from the plots of $(\alpha E)^{1/2}$ versus E_{Tauc} of 200 and 400 cycles (cycles).

indirect measurement method, and the obtained result could be a local minimum and not the global minimum. Hence, in order to confirm the reliability of our result, the above fit function is extrapolated to 1000 cycles and then the calculated thickness is supposed to be 98.23 nm. On the other hand, a sample has been deposited at 1000 cycles and its thickness has been examined using SEM. The derived thickness by SEM is 96.89 nm (see the inset in Figure 6), which indicates our SE analysis is reliable. Regarding the 1.34 nm thickness difference, it can be attributed to the following three reasons. First, the ALD growth speed is not constant in each cycle. Second, the thickness calculated by SE analysis has about 0.5 nm error. Third, the two thickness measurement methods, SE and SEM, have distinct principles, so there is an inherent difference in the results from them.

The optical band gap E_{TL} of Al_2O_3 has been extracted from the SE analysis. An obvious fluctuation of E_{TL} is not observed in all samples with different thickness. E_{TL} of five samples are ~3.0 eV, as shown in Table 2. Similarly, another optical measurement method, UV-VIS transmittance spectrum, is used to verify the obtained SE results. Figure 7 gives the UV-VIS transmittance spectra of samples in the wavelength range from 300 to 800 nm. The absorption coefficient α can be calculated from the transmittance spectra. The optical band gap is derived by Tauc plot. Generally, the Tauc equation can be expressed as

$$aE = A\left(E - E_{Tuac}\right)^n, \quad (5)$$

where A is a constant, E is the photon energy ($h\nu$), E_{Tuac} is the optical band gap, and n is the value decided by the transition process which is specifically divided into two kinds of situations: $n = 2$ for indirect transition and $n = 1/2$ for direct transition. The amorphous Al_2O_3 films have an indirect band gap, so $n = 2$ is adopted in this work.

According to the Tauc theory [12], the direct consequence of electron energy parabolic distribution is the linear feature of Tauc curve, so the band gap E_{Tauc} can be extracted from the linear extrapolation of curve to $\alpha E = 0$. As shown in Figure 8, the band gap E_{Tauc} of all samples is around 2.3 eV and has no significant fluctuation. The corresponding slope is near zero. This low slope is the same as the situation in SE measurement, which also convincingly verifies the reliability of our SE results. It is understandable because the amorphous Al_2O_3 films with different thickness have the identical atomic ratio Al/O as demonstrated by EDS. As to the difference between E_{TL} and E_{Tauc}, there are probably two reasons. First, the localization of electron wave functions and the subgap

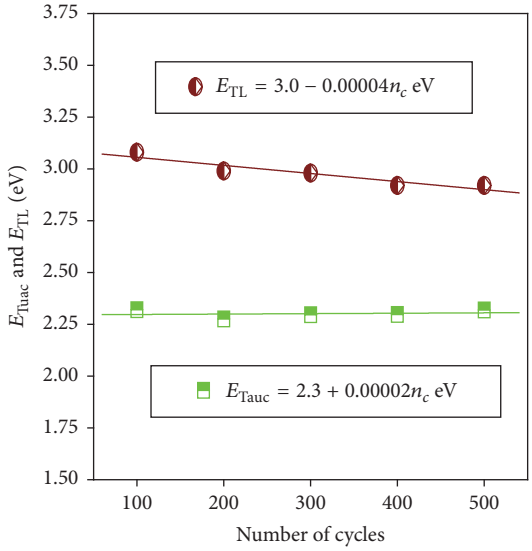

Figure 8: The optical band gap changes with the ALD cycles.

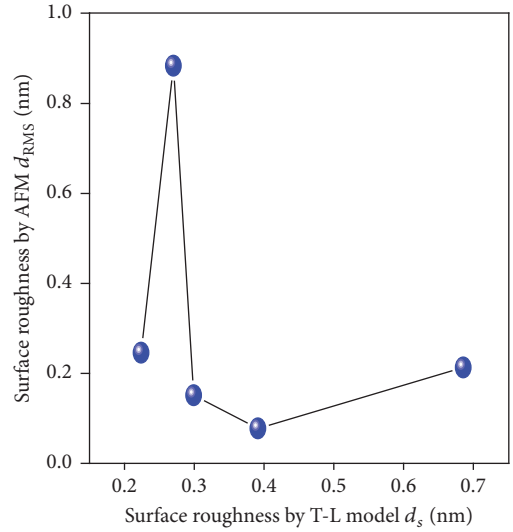

Figure 9: RMS roughness d_{rms} measured by AFM with tapping mode versus surface roughness d_s extracted from T-L model.

absorption in forbidden band is incorporated in Tauc model. However, the optical transition below band gap is zero by forcing $\varepsilon(E)$ to be 0 for $E \leq E_{TL}$ in the T-L model (see (5)). Second, in the UV-VIS measurement, only transmittance is recorded and other information, like polarization state, is lost.

Another important structural parameter extracted from SE analysis is the surface roughness d_s of thin film. As indicated by AFM measurement, d_s of all samples are relatively low, showing the good surface quality of Al_2O_3 thin film fabricated by ALD technology. d_{rms} from AFM measurement is found inconsistent with d_s from SE analysis. It is likely because of the different testing principle in the two methods. The AFM scanning process is a mechanical tapping method, which cannot detect the microstructure located below at surface, and the scanning area is micrometer level. In SE analysis, however, the surface roughness is a calculation outcome and the laser spot size is millimeter level. Further, the surface roughness is modeled as a mixture of 50% bulk Al_2O_3 layer and 50% voids based on EMA, which includes both the microstructure on surface and the microstructure in bulk layer. On the other hand, the relationship between d_s and d_{rms} is shown in Figure 9. An apparent mathematical relationship between the two sets of value cannot be found. This is different from the report of Koh et al. [20] in 1996, where an obvious linear relationship is observed in amorphous Si_xC_{1-x}:H thin film. It could be ascribed to the different testing material.

The refractive index n and extinction coefficient k are also the key parameters to characterize the optical properties of amorphous Al_2O_3 films with different thickness. As shown in Figure 10(a), the n/k value of Al_2O_3 films is calculated based on the obtained SE fitting parameters. Result shows that n/k value of samples is dependent on film thickness. It exhibits a similar variation trend, which increases with different thickness. The sample with 500 cycles has the maximum n/k values and the sample with 100 cycles has the minimum ones. At 400 nm wavelength, n increases from 1.536 to 1.721 with the thickness increasing from 11.62 nm to 50.40 nm. The inflection point at ~400 nm wavelength (~3 eV) in k curves means the onset of optical absorption, which is in agreement with the above results. The surface defects may exist in the films, including the stress and strain change or the imperfect crystal. This surface defect of Al_2O_3 films in the ALD is determined by the number of activation groups and saturation adsorption capacity. The thicker samples may exhibit stress and strain, and thinner films may have amorphous phase [21]. The ratio of defects and the volume ratio of air have an effect on the film surface with different thickness. The n/k values can be improved by the thickness variation of films [22]. Meanwhile, the interfacial layer always has influence on the n/k values of the Al_2O_3 samples, because the refractive index and the layer thickness in any layer have a direct influence on analysis result according to the Snell law and transfer matrix. As the films thickness increases, the defects may be decreased, the values of n/k tend to be similar with the Al_2O_3 bulk layer. However, the influences are inevitable resulting from the interfacial layer. In our work, the interfacial layer plays a main role in the n/k values of Al_2O_3 samples and the roughness of the surface was subordinate. These results demonstrate that thickness plays an important role in the optical properties of Al_2O_3 thin films.

The absorption coefficient also can be calculated from analysis through the relationship $\alpha = 4k\pi/\lambda$ [23]. It can be seen that the increased film thickness enhance the absorption capacity of materials.

The electronic response of material depends on its dielectric function, which reflects the interaction between the electrons and the applied field in materials. Figure 11 provides the calculated dielectric function spectra of amorphous Al_2O_3 film with different thickness. It can be observed that the spectra display a systematic change with the increase of cycles. For all Al_2O_3 film samples, the value of $\varepsilon_2(E)$ is zero when the photon energy is between 0 and E_{TL} (~3.0 eV),

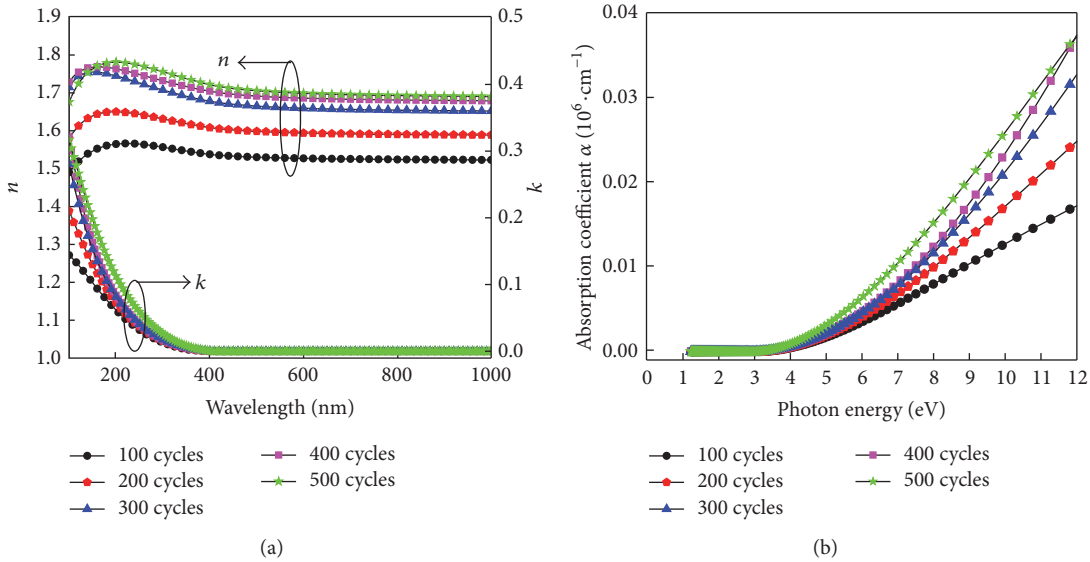

FIGURE 10: (a) Refractive index n (continued curves) and extinction coefficient k (open symbols) spectra derived from the Al_2O_3 films with different thicknesses. (b) Absorption spectra of Al_2O_3 films with different thickness.

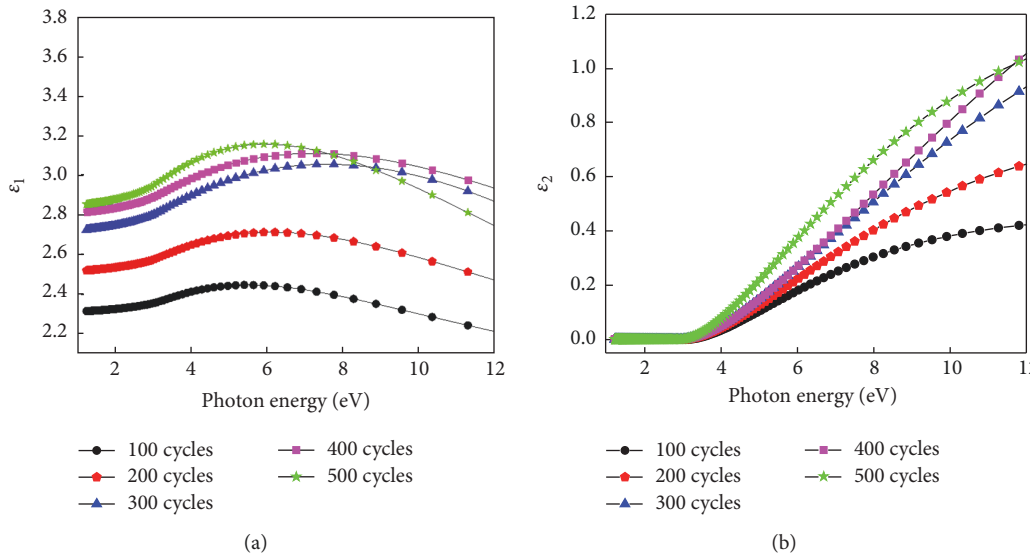

FIGURE 11: The dielectric functions of Al_2O_3 films with different thickness samples by the T-L model: real part (a) and imaginary part (b).

because the electron transitions less than E_{TL} are forbidden in the Tauc-Lorentz mode [24]. The nonzero value of the curve front end shows the occurrence of the absorption of Al_2O_3 films, and the boundary point of zero and nonzero values is the optical band gap.

4. Conclusions

In summary, the amorphous ALD-Al_2O_3 films with various thicknesses are successfully fabricated at 200°C. The XRD and EDS measurements show that the films were amorphous structure and stable O/Al ratio. The AFM indicates that the surface morphologies of all samples are smooth and crack-free with similar surface roughness values. The SE analysis reveals that the film thickness increases regularly with the increase of ALD cycles, corresponding to a growth rate of ~0.1 nm/cycle. Further analysis on SE and UV-VIS transmittance spectrum shows that the band gap E_{TL}/E_{Tauc} of all samples is ~2.3 eV/3.0 eV, with no significant fluctuation. n/k of ALD-Al_2O_3 films are related to their bulk layer thickness. The bulk layer plays a key role in the n/k values of Al_2O_3 samples, and the surface roughness is subordinate. The outstanding performances stem from the constructed amorphous thin films. Considering the easy fabrication and excellent performances, this method can be used broadly to deposit other amorphous minerals, and this structure will be promising in practical application for other optoelectronic film materials deposition, especially Ti/Fe/Zn oxides deposition.

Abbreviations

ALD: Atomic layer deposition
EDS: Energy dispersive spectrum
XRD: X-ray diffraction
AFM: Atomic force microscopy
SE: Spectroscopic
Al_2O_3: Aluminum oxide
TMA: Trimethylaluminum
T-L: Tauc-Lorentz
F-B: Forouhi-Bloomer
RMS: Root mean square
RMSE: Root mean square error.

Conflicts of Interest

No potential conflicts of interest were reported by the authors.

Acknowledgments

This work is supported by the National Natural Science Foundation of China (Grants nos. 51605449, 51422510, 51675493, and 61471326), Shanxi Province Applied Fundamental Research Program (201601D021064), the National High Technology Research and Development (863) Program of China (Grant no. 2015AA042601), and Shanxi "1331 Project" Key Subject Construction (1331KSC).

References

[1] J. Houska, J. Blazek, J. Rezek, and S. Proksova, "Overview of optical properties of Al_2O_3 films prepared by various techniques," *Thin Solid Films*, vol. 520, no. 16, pp. 5405–5408, 2012.

[2] C. Bjormander, "CVD deposition and characterization of coloured Al_2O_3/ZrO_2 multilayers," *Surface and Coatings Technology*, vol. 201, no. 7, pp. 4032–4036, 2006.

[3] S. K. Shamala, C. S. L. Murthy, and N. K. Rao, "Studies on optical and dielectric properties of Al_2O_3 thin films prepared by electron beam evaporation and spray pyrolysis method," *Materials Science & Engineering B*, vol. 106, no. 3, pp. 269–274, 2004.

[4] G. Angarita, C. Palacio, M. Trujillo, and M. Arroyave, "Synthesis of alumina thin films using reactive magnetron sputtering method," *Journal of Physics: Conference Series*, vol. 850, no. 1, Article ID 012022, 2017.

[5] B. Hu, M. Yao, R. Xiao, J. Chen, and X. Yao, "Optical properties of amorphous Al_2O_3 thin films prepared by a sol-gel process," *Ceramics International*, vol. 40, no. 9, pp. 14133–14139, 2014.

[6] C. Cibert, H. Hidalgo, C. Champeaux et al., "Properties of aluminum oxide thin films deposited by pulsed laser deposition and plasma enhanced chemical vapor deposition," *Thin Solid Films*, vol. 516, no. 6, pp. 1290–1296, 2008.

[7] R. W. Johnson, A. Hultqvist, and S. F. Bent, "A brief review of atomic layer deposition: from fundamentals to applications," *Materials Today*, vol. 17, no. 5, pp. 236–246, 2014.

[8] S. M. George, "Atomic layer deposition: an overview," *Chemical Reviews*, vol. 110, no. 1, pp. 111–131, 2010.

[9] P. C. Snijders, L. P. H. Jeurgens, and W. G. Sloof, "Structural ordering of ultra-thin, amorphous aluminium-oxide films," *Surface Science*, vol. 589, no. 1-3, pp. 98–105, 2005.

[10] A. Khanna, D. G. Bhat, A. Harris, and B. D. Beake, "Structure-property correlations in aluminum oxide thin films grown by reactive AC magnetron sputtering," *Surface and Coatings Technology*, vol. 201, no. 3-4, pp. 1109–1116, 2006.

[11] H. Fujiwara, *Spectroscopic Ellipsometry: Principles and Applications*, John Wiley & Sons, 2007.

[12] H. G. Tompkins and E. A. Irene, *Handbook of Ellipsometry*, Springer, 2005.

[13] A. R. Forouhi and I. Bloomer, "Optical dispersion relations for amorphous semiconductors and amorphous dielectrics," *Physical Review B: Condensed Matter and Materials Physics*, vol. 34, no. 10, pp. 7018–7026, 1986.

[14] L. Canham, *Handbook of Porous Silico*, Springer International Publishing, 2014.

[15] J. D. Ferguson, A. W. Weimer, and S. M. George, "Atomic layer deposition of Al_2O_3 films on polyethylene particles," *Chemistry of Materials*, vol. 16, no. 26, pp. 5602–5609, 2004.

[16] T. O. Kääriäinen and D. C. Cameron, "Plasma-assisted atomic layer deposition of Al_2O_3 at room temperature," *Plasma Processes and Polymers*, vol. 6, no. 1, pp. S237–S241, 2009.

[17] K. Gupta and T. A. Saleh, *Sale: Carbon Nanotubes—From Research to Applications, Chapter 17*, InTech, 2011.

[18] E. Langereis, S. B. S. Heil, H. C. M. Knoops, W. Keuning, M. C. M. Van De Sanden, and W. M. M. Kessels, "In situ spectroscopic ellipsometry as a versatile tool for studying atomic layer deposition," *Journal of Physics D: Applied Physics*, vol. 42, no. 7, Article ID 073001, 2009.

[19] Q.-Y. Cai, Y.-X. Zheng, D.-X. Zhang et al., "Application of image spectrometer to in situ infrared broadband optical monitoring for thin film deposition," *Optics Express*, vol. 19, no. 14, pp. 12969–12977, 2011.

[20] J. Koh, Y. Lu, S. Kim, J. S. Burnham, C. R. Wronskiand, and R. W. Collins, "Real time spectroscopic ellipsometry study of hydrogenated amorphous silicon p-i-n solar cells: Characterization of microstructural evolution and optical gaps," *Applied Physics Letters*, vol. 67, p. 2669, 1995.

[21] Z.-Y. Wang, R.-J. Zhang, H.-L. Lu et al., "The impact of thickness and thermal annealing on refractive index for aluminum oxide thin films deposited by atomic layer deposition," *Nanoscale Research Letters*, vol. 10, no. 1, 2015.

[22] Q. Y. Cai, Y. Zheng, P. Mao et al., "Evolution of optical constants of silicon dioxide on silicon from ultrathin films to thick films," *Journal of Physics D: Applied Physics*, vol. 43, no. 44, Article ID 445302, 2010.

[23] J. N. Hilfiker, N. Singh, T. Tiwald et al., "Survey of methods to characterize thin absorbing films with Spectroscopic Ellipsometry," *Thin Solid Films*, vol. 516, no. 22, pp. 7979–7989, 2008.

[24] Z. Xu, F. Zhang, R. Zhang et al., "Thickness dependent optical properties of titanium oxide thin films," *Applied Physics A: Materials Science & Processing*, vol. 113, no. 3, pp. 557–562, 2013.